AD-A184 431 AFAR (AZORES FIXED ACOUSTIC RANGE) MEASUREMENTS OF INTENSITY AND INTENSITY MOMENTS(U) CALIFORNIA UNIV SANTA CRUZ DEPT OF PHYSICS S M FLATTE ET AL SEP 86 1/1

UNCLASSIFIED F/G 20/1 NL

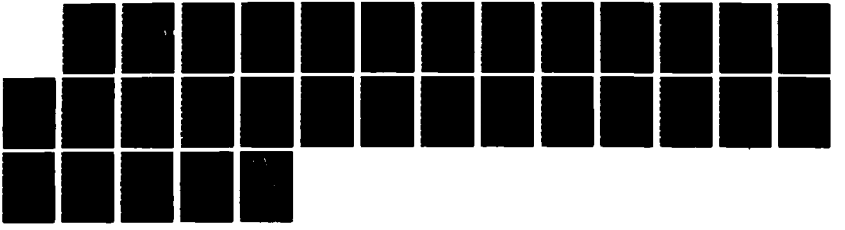

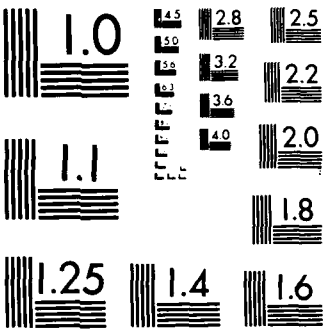

MICROCOPY RESOLUTION TEST CHART
NATIONAL BUREAU OF STANDARDS-1963-A

AFAR measurements of intensity and intensity moments

by

Stanley M. Flatté[a]

Stephen A. Reynolds[a]

Physics, University of California
Santa Cruz, CA *95064*

Roger Dashen

Physics, University of California
San Diego, CA *92093*

Barry Buehler
and
Pat Maciejewski

Naval Underwater Systems Center
New London, Connecticut, *06320*

September 1986

[a] Presently at the Applied Physics Laboratory, University of Washington, Seattle, WA 98105

September 1986

ABSTRACT

In an acoustic-oceanographic experiment (AFAR) performed near the Azores in 1975, frequencies from 400 to 4670 Hz were transmitted over a 35-km wholly refracted path. In addition, a separate data set was gathered over a 3-km path in 1973. Measurements of the intensity coherence function of time and frequency, intensity moments, and the probability distribution of intensity are presented and compared with predictions of fluctuations due to internal waves.

December, 1986

INTRODUCTION

In this paper we compare with theory some observations made by Ellinthorpe[1,2] of the statistics of acoustic intensity observed at the Azores Fixed Acoustic Range (AFAR). We treat two separate experiments, one in 1973 and a second in 1975. Our theoretical predictions for the intensity statistics are obtained from the path-integral formulation under the assumption that the effects of internal waves dominate the acoustic fluctuations. This approach is presented in Dashen[3] and Flatté et al,[4] and reviewed in Flatté.[5] A companion paper[6] presents the pertinent theoretical considerations relevant to the comparison between the predictions and observations of intensity at AFAR. In an earlier pair of papers [7,8] a similar comparison for the second moment (mutual coherence function) and a detailed description of environmental observations were given. Here, we present the fourth moments (more specifically $<I(0)I(\Delta t)>$ and $<I(0)I(\Delta\sigma)>$, where Δt and $\Delta\sigma$ are separations in time and frequency, and the scintillation indices); higher moments; and probability distributions.

It is now accepted that ocean acoustic fluctuations having time scales from minutes to days are caused predominantly by internal-wave-induced oceanic variability in the sound-speed field.[5] Ocean experiments have sampled the fluctuating acoustic intensity field at a variety of locations and ranges. Adopting the $A-\Phi$ scattering parametrization, we note three regions that catagorize acoustic fluctuations (Figure 1). In the unsaturated regime ($A\Phi^2<1$ or $\Phi<1$), where the intensity field is expected to obey log-normal statistics, there are no experiments. Both the San Clemente experiment,[9] and the experiments at Cobb Seamount [10,11] are near the $A\Phi^2=1$ boundary. All these experiments found stronger intensity fluctuations than one would expect over a weakly scattered, unsaturated path. In the saturated regime ($A\Phi>1$) where the complex field components are expected to be Gaussian, there are the MIMI experiments,[4,12,13] and an experiment southwest of Bermuda.[14] The ENACEX observations[15] sampled three ranges with a frequency of 460 Hz and several paths and thus sampled a broad range in $A\Phi$-space. ENACEX was used to estimate several fluctuation parameters directly from the measurements. The paths predicted to be nearly saturated exhibited partially saturated behavior. Since the time of these experiments, the path-integral theory has developed sufficiently so that intensity observations where the environment is adequately known can be used to test theoretical predictions with greater precision.

The AFAR propagation occurred over two paths, one of nearly 3 km in 1973 and a fixed path of 35 km during 1975. These observations, for the several center frequencies transmitted at each range, place the short range experiment in the unsaturated regime

and the 35 km path in partial saturation (Figure 1). Simultaneously with the 1975 experiment, an extensive set of environmental measurements were made.

The paper is divided into three parts. Part I reviews, from our earlier paper, the acoustic experiments and the oceanographic observations determining the parameters of the internal-wave model (we use the GM-formalism).[11] We also introduce the theoretical framework discussed in our companion paper.[6] The intensity measurements and the fourth moments are presented in Part II and the probability densities and higher moments in Part III. The paper concludes with a summary: Part IV.

I. EXPERIMENT REVIEW AND OVERVIEW OF THEORY

A brief overview of the experiment is presented here. The interested reader may find more experimental detail and an associated list of references in our earlier paper.[8] Several different frequencies were transmitted over each of two refracted paths from a fixed transmitter at 540-m depth located west of Santa Maria Island in the Azores. A 2798-m path (inclined upward at 5 degrees) was monitored for seven hours in November 1973; the receiver was a hydrophone suspended at 325-m depth beneath a trimooring. Three pulses having center frequencies 749.8, 1499.8 and 2800.0 Hz were transmitted every 1.048576 s. A longer 35026-m path was monitored with a fixed receiver located at 736-m depth for over 186 h beginning in March 1975, simultaneously with an extensive oceanographic experiment. Three 130 ms-pulses of 412.46, 1012.33 and 4673.01 Hz, and a fourth 1.25-ms 3199.5-Hz pulse, all having Gaussian envelopes, were transmitted at a 10.15808-s repetition interval. In the language of communication theory, the short pulse is used to measure the channel frequency response and the long pulse measures the time response.

Environmental measurements obtained during the 1975 experiment determine the background sound-speed field and the parameters of the Garrett-Munk (GM) internal-wave model.[16] The sound-speed profile has a minimum near 714 m in addition to the deeper SOFAR axis. The intervening maximum near 850 m, is caused by the intrusion of Mediterranean water. The 714-m minimum creates a duct for the long-range ray, which has two turning points and two caustics.[8] Specification of the internal-wave field involves parametrization of the rms vertical displacement ς_0, bandwidth j_*, and the scaling parameter n_0B of the dispersion relation. Using a combination of horizontal, vertical, and temporal environmental data, values for the parameters were obtained [8] of $n_0B = 3.0$ cph-km, $\varsigma_0 = 13.1$ m and $j_* = 3$. These are the same as the canonical GM model with the important exception that ς_0, the parametrization of the internal-wave energy level, is much larger than the canonical value of nearly 7 m and is relatively high compared with other oceanic internal-wave observations.[17] For our purposes this means AFAR is a good place to study internal-wave-induced acoustic fluctuations.

With the model sound-speed statistics specified, then the theoretical predictions for the intensity statistics can be obtained for the AFAR site. The companion paper addresses the derivation of the expressions using the path-integral formalism.[6] The theoretical quantities of interest include the intensity correlation function in time $K(\Delta t)$ and the micropath bandwidth function $Q(\Delta\sigma)$ from which the intensity correlation of frequency is obtained. For these quantities the comparison between observations and theory is contained in the following intensity correlations:

$$r(\Delta t) \equiv 2\cdot\frac{<I(\Delta t)I(0)>}{<I(0)I(0)>} - 1 = K(\Delta t), \tag{1}$$

and

$$r(\Delta\sigma) \equiv 2\cdot\frac{<I(\Delta\sigma)I(0)>}{<I(0)I(0)>} - 1 = |\,Q(\Delta\sigma)\,|^2 \tag{2}$$

where the brackets $<>$ indicate an average over the duration of the experiment, which is taken to represent an ensemble average over the statistical internal-wave field. (The mean intensity is by definition equal to unity.) The solution of $K(\Delta t)$ involves numerical integration of a second-order differential equation along the equilibrium ray, as described in the companion paper.[6] The theory for Q was described earlier.[7]

In full saturation, $K(\Delta t) = e^{-D(\Delta t)}$ and for small time lags, $D(\Delta t) \approx (\nu\Delta t)^2$.[4] In an analogous manner, in the partially saturated regime, an expression for K can be defined for small time lags,

$$K(\Delta t) \approx e^{-(\nu'\Delta t)^2}. \tag{3}$$

This defines an intensity decorrelation time scale $1/\nu'$, which can be calculated by means of ordinary integrals along the ray from source to receiver, for given internal-wave parameters.[6]

The behavior of $|Q(\Delta\sigma)|^2$ can be approximated for some purposes by

$$|\,Q(\Delta\sigma)|^2 \approx e^{-(\tau_0\Delta\sigma)^2} \tag{4}$$

where τ_0 can be calculated by means of ordinary integrals along the ray as well, again if the internal-wave field is quantitatively characterized.[8]

For the moments of intensity, as shown by Dashen[18] the general asymptotic form is:

$$<I^N> = N!\exp\left[\frac{(N(N-1))}{2}\gamma f_2(\gamma) - \frac{N(N-1)(N-2)}{3!}\gamma^2 f_3(\gamma) + \cdots\right] \tag{5}$$

The form of (5) for small γ with $f_2(\gamma) = 1$ is used here:

$$<I^N> = N!\exp\left[\frac{N(N-1)}{2}\gamma\right] \tag{6}$$

where the value for γ is obtained from the effects of internal waves by the path-integral technique.[19] For small γ, (6) takes on the more familiar form

$$<I^N> = N!\left[1 + \frac{N(N-1)}{2}\gamma\right] \tag{7}$$

The moments obtained from the K-distribution[20] are also considered, where we use the form

$$\langle I^N \rangle = N! \frac{\Gamma(N + 1/\gamma)\gamma^N}{\Gamma(1/\gamma)} \tag{8}$$

Not only the solutions $K(\Delta t)$ and $Q(\Delta t)$ but also all other quantities including ν, ν', τ_0 and γ are obtained by numerical integrations along the deterministic, background ray from source to receiver. The AFAR background ray path is calculated using a sound-speed profile obtained from an average of 65 STDSV casts taken during the 1975 field experiment. There is an issue of determining the mean background profile and distinguishing it from the fluctuating profile. Even with the formation of an average profile from many casts, the intensity related quantities including K, A, and Q are functions of how the background profile is smoothed. The smoothing (and interpolation) algorithm used here is a cubic spline technique,[21] involving a parameter which is the rms deviation of the smooth profile from the measured points. The predictions are sensitive to this parameter, as was described in our earlier paper[8] involving Q. For the comparison with AFAR the smoothing parameter is, unless specified, set to 1 cm/s. This level of smoothing effectively filters out much of the high vertical wavenumber variability (smaller than 20 m) from the background sound-speed profile.

II. FOURTH MOMENTS

In treating the statistics of any time series it is useful to initially examine the character of the series. This is helpful at AFAR where there are intensity measurements from experiments in two quite different scattering regimes. Figure 2 shows time series from three frequencies at each of the two ranges. The entire available data set is shown for the 2.8-km path; 20 h of data (an inertial cycle at the AFAR latitude) is shown from the 35-km path. Note that the short-path intensity ordinate is a factor of 2 smaller than that for the longer path.

Over the shorter path, the data series from the different frequencies display the same general oscillation sequence in time. As the acoustic frequency increases, the oscillations increase in amplitude. This is the behavior expected in a weak, geometric regime, where theoretically the scintillation in log-intensity scales with frequency. The observed scintillation indices for log-intensity (and intensity) are 0.10 (0.10), 0.21 (0.15), and 0.59 (0.34) for 750, 1500, and 2800 Hz respectively.

Over the 35 km path, at longer time scales, the data behave in a similar manner. For example there is a broad increase in intensity centered about 10 hours and again

after 16 hours. However, comparing the shorter-time-scale events oscillating inside the long period envelopes, the three series are quite different and the high intensity spikes between frequencies are often not in alignment. Over very short time scales the series for the different frequencies are quite different. The observed scintillation indices of intensity for the 35 km path are 1.24, 1.21, and 1.47, for 410, 1010, and 4670 Hz respectively. The corresponding log-intensity variances are 1.8, 1.7, and 1.9. These are above the saturation limit of 1 for intensity and 1.66 (5.6 dB) for log-intensity. This is the behavior characteristic of partial saturation, in which the deterministic ray has been broken apart into many microrays by the internal-wave fluctuations. The level of scintillation at 4670 Hz is higher than expected on a curve asymptotically approaching 1 from above. (The approach to 1 is very gradual in partial saturation.)

We turn now to the comparison of the observed fourth moments (intensity correlations) and theory. A quantitative examination is made of the observations over the 35-km path. Because of mooring-motion problems, the 2.8 km path cannot be used with the intensity correlation studies. The temporal correlation function $r(\Delta t)$ for 1010 Hz is plotted in Figure 3. Standard FFT techniques[22] for the correlation functions are used and the confidence limits are obtained from the equations in Appendix B of Spiesberger and Worcester.[14]

The prediction $K(\Delta t)$ is a function of smoothing of the background sound-speed profile. $K(\Delta t)$ curves for two smoothings, 1 and 1.5 cm/s, are shown in Figure 3; 90% confidence intervals are shown for a few lags on the dotted data curve. As one might expect, the greater the smoothing, the more slowly the predicted correlation function falls with lag. There is a smooth transition from no smoothing through 1 cm s^{-1} to the 1.5 cm s^{-1} curve. Further smoothing does not significantly change $K(\Delta t)$ from the curve shown for 1.5 cm s^{-1}. In what follows the theoretical results obtained using a smoothing equal to 1 cm s^{-1} are given. This smoothing approximately removes from the sound-speed profile variations at scales less than a Fresnel zone size at AFAR ($\approx$ 20 m) and so the selection of the 1 cm s^{-1} scale is not entirely arbitrary. The sensitivity of the intensity results to the profile smoothing remains an important problem.

Also shown in Figure 3 is the approximation to $K(\Delta t)$ given by (3). The decorrelation scale, ν', is obtained from equation (44) of our companion paper.[8] The data appear to follow the Gaussian form of (3), with perhaps a slightly higher value of ν', at least as well as the form of $K(\Delta t)$ from more elaborate calculations. Since there are environmental uncertainties in the calculation of ν', we feel that we cannot, from the correlation-function data, distinguish between $K(\Delta t)$ and its Gaussian approximation. Another approximation for K (Δt); that is, $|Q|^2$ from (40) of our companion paper, is

shown as well. If the prediction for $K(\Delta t)$ in full saturation is used

$$K(\Delta t) = \exp\left[-(\nu \Delta t)^2\right] \tag{9}$$

there would be a substantial disagreement with data, since ν is substantially larger than ν' (see Table 1). In Figure 4, the observed correlation functions, $r(\Delta t)$, are plotted for three acoustic frequencies, with 90% confidence intervals for a few lags. The observed intensity decorrelation times are 0.56, 0.13, and 0.03 h for 410, 1010, and 4670-Hz respectively. Overplotted as solid curves are the $K(\Delta t)$ predictions (1 cm/s smoothing). At the 90% confidence level the theoretical curves are in agreement with the observations over much of the range in correlation and the comparisons are in general quite good. The $K(\Delta t)$ curves at different frequencies are related by a simple time scaling that is proportional to $\sigma(\ln\Phi)^{1/4}$ with σ the acoustic frequency. The predicted behavior of $K(\Delta t)$ with both Δt and acoustic frequency is as observed.

The power spectrum and the correlation function are Fourier transform pairs and we now turn to consider the observations in the frequency domain. Note that $r(\Delta\sigma)$ is not a transform pair with the curves in Figures 4; it is the correlation of intensity as a function of frequency lag and is treated later.

The power spectra of the observed 35-km intensity time series $P_I(\omega)$ are plotted in Figure 5. Standard FFT-techniques were used.[22] These spectra were obtained by normalizing the series to a mean intensity of unity and then averaging spectra from 50% overlapping 23.12-h segments. A missing 5.6-h segment in the 4670-Hz data was filled using linear interpolation. Each segment was mean-zeroed and filtered with a cosine taper to reduce leakage. The spectra obtained from the segment averages were bin averaged over 0.05 logarithmic intervals in frequency ω (to avoid confusion with acoustic frequency σ, the temporal transform variable ω is used in the text); 90% confidence intervals are shown. The observed spectra have been multiplied by $2/<I^2>$ so that a comparison can be made with the Fourier transform of $K(\Delta t)$. (The integrals of the spectra are equal to two.)

The observed spectra have an $\omega^0 - \omega^{-1}$ dependence at low ω. At a higher ω (which is dependent on acoustic frequency) the spectra begin to roll off. The acoustic-frequency dependent break in slope in the power spectrum has also been observed elsewhere.[11] There appear to be possible influences from the semidiurnal tide ($\omega = .08$ cph) appearing as a bulge at low ω in the 4670-Hz intensity spectrum. The spectra in Figure 5 were calculated in a way meant to remove the longer period variability and so low-frequency lines are smeared. At large ω, the noise floors are four to five decades below the energy containing parts of the spectra.

The predictions obtained from the Fourier transform of $K(\Delta t)$ are overplotted in Figure 5. The behavior in ω and acoustic-frequency σ is very similar to the observations. The measured spectra fall below the predicted curves at high ω. Because the high-ω tail is sensitive to the smoothing parameter this is not felt to be a failure in the theory.

To see the distribution of spectral energy with ω consider the variance preserving plots shown in Figure 6. Equal areas under the curves contain equal contributions to the integral of the spectrum. The theoretical curves match the observations except very near the maxima. They are within a factor of two of the observations of the distribution of the fourth moment in ω. The peak in the 410 Hz spectrum at 0.3 cph is not significantly different from the prediction at the 90% confidence level. Finally, we remark that the theoretical predictions for Figures 5 and 6 would not be significantly different if the Gaussian approximation (3) for $K(\Delta t)$ were used, if slight adjustments in the values of ν' were allowed.

The intensity correlation in frequency $r(\Delta\sigma)$, given by (2), is plotted in Figure 7. The short 1.25-ms, 3199-Hz pulses were used to estimate $r(\Delta\sigma)$. Each pulse was Fourier transformed and it's spectrum calculated and then normalized by the average of the pulse spectra observed over the entire 187 h experiment. A correlation function in frequency was then obtained from each normalized pulse spectrum and averaged over all pulses. The result is plotted in Figure 7 with the prediction obtained from $|Q(\Delta\sigma)|^2$. The comparison is quite good down to a level less than 0.2 in $r(\Delta\sigma)$. Also shown is the Gaussian approximation to $|Q|^2$ from (4).

Of interest is another fourth moment that, like $r(\Delta\sigma)$, uses the theoretical quantity $|Q(\Delta\sigma)|^2$ for prediction; it is the intensity-lagged correlation given by

$$f(\tau) = <\int_{-\infty}^{\infty} I(t+\tau)I(t)dt> / <\int_{-\infty}^{\infty} I^2(t)dt> \qquad (10)$$

The lagged correlation coefficient of intensity is formed for each 1.25-ms pulse at 3200 Hz. The average $f(\tau)$ is then obtained by averaging the correlations from all pulses and normalizing by the value at lag $\tau = 0$. Note that unlike $I(\tau)$,[8] $f(\tau)$ does not depend upon the pulse arrival time and so does not contain the wander of the pulse in time.

The prediction for $f(\tau)$ requires knowledge of the transmitted pulse; equation (15) of Worcester, Williams and Flatte'[9] is used.

$$f(\tau) = \frac{1}{2\pi}\int\int_{-\infty}^{\infty}\int d\Delta\sigma d\sigma d\sigma' P(\Delta\sigma,\sigma,\sigma')[\,|Q(\Delta\sigma)|^2 + |Q(\sigma-\sigma')|^2]e^{i\Delta\sigma\tau} \qquad (11)$$

where

$$P(\Delta\sigma,\sigma,\sigma') = X(\sigma + \frac{\Delta\sigma}{2})\, X^*(\sigma - \frac{\Delta\sigma}{2})\, X(\sigma' + \frac{\Delta\sigma}{2})\, X^*(\sigma' - \frac{\Delta\sigma}{2}) \qquad (12)$$

The transmitted pulse shape was a Gaussian given by $x(\tau) = e^{(-\frac{\tau^2}{2\alpha^2})}$ so that

$$X(\sigma) \propto e^{(-\frac{\alpha^2\sigma^2}{2})} \qquad (13)$$

where $\alpha = 0.53$ ms.

Substituting (13) into (12) and (11) gives

$$f(\tau) = \tfrac{1}{2}\left\{\frac{g(\tau)}{g(0)} + e^{-\frac{\tau^2}{2\alpha^2}}\right\} \qquad (14)$$

where

$$g(\tau) = \int_{-\infty}^{\infty} dv\, |Q(v)|^2 \exp\left\{-\tfrac{1}{2}\alpha^2 v^2 + i v \tau\right\} \qquad (15)$$

The first term in (14) depends on the medium-induced pulse spreading, represented by the Q function. The second term is a replica of the transmitted pulse. Note that at $\tau = 0$ the two terms contribute equal amounts. We may get some idea of the behavior of $f(\tau)$ by using the approximation for $|Q|^2$ in (4); this yields

$$f(\tau) = \tfrac{1}{2}\left\{\exp\left[-\frac{\tau^2}{2\alpha^2 + 4\tau_0^2}\right] + \exp\left[-\frac{\tau^2}{2\alpha^2}\right]\right\} \qquad (16)$$

Thus, if $\tau_0 \ll \alpha$, $f(\tau)$ is a replica of the transmitted pulse. If $\tau_0 \gg \alpha$, then $f(\tau)$ has a replica of the transmitted pulse sitting on top of a much wider Gaussian with rms spread of $1.4\,\tau_0$.

However, (3) is not a good approximation for the tail of $f(\tau)$, because that tail is dominated by the low-lying eigenvalues discussed in reference 8. Thus $g(\tau)$ must be calculated numerically for AFAR. This has been done, and the result is shown in Figure 8. Thus intensity measurements can be used to measure the effect of these low-lying eigenvalues, and $|Q|^2$ cannot be characterized by τ_0 only.

III. PROBABILITY DISTRIBUTIONS AND MOMENTS

For the 2.8-km data series the expectation is that the log-intensities are normally distributed. The time series of log-intensity were divided into 35-minute segments with each segment normalized to have a mean intensity of unity. The log-intensities from each segment were then binned to form histograms. From an average of the histograms the probability densities were calculated for each acoustic frequency with the results plotted in Figure 9. This technique removed dominant oscillations at low frequency in the 7 hour data set at 750 Hz. There is very little difference in the 1500 and 2800 Hz distributions whether short or long segments are used. The confidence intervals are calculated using the technique given in Appendix B of Spiesberger and Worcester.[14] In general, the 2.8 km log-intensities are normally distributed as expected. A normal distribution is overplotted for each series with the mean and variance given by the observed distributions.

The observed probability density functions for three frequencies from the 35-km range, are shown in Figure 10. The axes are log-linear so that an exponential would be a straight line. Below the 10^{-3} level in probability the 90% confidence intervals are quite large due to the small number of observations. Note that the confidence intervals at small intensity for 410 Hz are broader than for 4670 because of the longer correlation times in the 410 Hz series. The data fall nearly linearly in probability space for almost two decades and then lead into a tail that becomes more prominent with increasing acoustic frequency. This is the behavior modeled by the K-distribution,[20] shown as solid curves in Figure 10. The parameter of the distribution is the normalized intensity variance, which is obtained from the $<I^2>$ values given in Table 2. In all cases, the data are well represented by a K-distribution with the observed intensity variance.

The observed intensity variances are 1.24, 1.21, and 1.47 for 410, 1010 and 4670 Hz. The 4670-Hz scintillation is higher than expected. The values predicted for γ, 0.15, 0.11 and 0.064 give intensity variances of 1.3, 1.22, and 1.13 for 410, 1010, and 4670 Hz respectively. Agreement between theory and experiment is reasonable at 410 and 1010 Hz. The cause of the disagreement at 4670 Hz is unknown, although it is known that γ is sensitive to the shapes of the profiles in sound speed and buoyancy frequency.

The observed normalized moments of intensity, $<I^N>/<I>^N$, for $N = 2$ to 6 are given in Table 2 for 410, 1010, and 4670 Hz. The observed moments increase faster with N than $N!$, (the prediction of an exponentially distributed intensity series in full saturation). The predictions for the moments obtained from (6) and (7) are tabulated as well as those obtained using the moments of the K-distribution (8), where each prediction

has been normalized to have the correct second moment.

It is very difficult to estimate errors on these moment determinations, because the error on $<I^N>$ depends on the true value of $<I^{2N}>$ which is very uncertain when N is large. The approximate numbers of independent observations of intensity, based on experiment duration divided by the intensity correlation time, $1/\nu'$, are 720, 2200, and 12,600 for 410 Hz, 1010 Hz, and 4670 Hz, respectively. As an example of the uncertainty in the moment error, consider $<I^5>$. If the intensity probability distribution were exponential the error in this moment at 4670 Hz would be 18; if the K-distribution applied, the error would be 2000; if the K-distribution applied, but the dynamic range of the experiment were limited at an intensity of twelve times the mean, then the error would be about 200. Thus, within the roughly estimated errors, all the one-parameter models considered fit the data reasonably well. Extending to a 2-parameter empirical model such as that given by Macaskill and Ewart,[23] as they point out, does not seem necessary to fit the AFAR data.

IV. SUMMARY AND CONCLUSIONS

We have compared observations of acoustic fluctuations in intensity at AFAR with the theory of acoustic propagation through internal waves. The predictions are sensitive to small changes in the sound channel, but knowledge of the sound channel and the internal-wave field was sufficiently precise to achieve good agreement for the intensity coherence functions of time and of acoustic frequency, as well as their corresponding spectra. The behavior at small time lag is governed by a parameter ν' that can be calculated from a double integral along the ray from source to receiver, and the observations agree with the calculated ν'. The intensity coherence of acoustic frequency is grossly characterized by a parameter τ_o that can be calculated in a manner similar to ν'.

The probability density of intensity has been observed at two ranges, one in the unsaturated region and the other in the partially saturated region. The former fits a log-normal distribution and the latter fits a K-distribution. The distribution in the partially saturated region is characterized by the microray focussing parameter γ. Calculation of γ from the internal-wave spectrum is very sensitive to the sound-speed profile, so that reliable predictions could not be made at AFAR.

We are grateful for a number of useful conversations with Dennis Creamer and Frank Henyey of CSND, and for the hospitality of the La Jolla Institute, where some of this work was done. This work was supported by the Office of Naval Research.

1. A. W. Ellinthorpe, "The Azores Range," Technical Document 4551, NUSC, New London, CT, 11 April 1973.

2. B. G. Buehler, "Volume propagation experiments at the Azores Fixed Acoustic Range," Technical Report 5785, NUSC, New London, CT, 21 Sept 1979.

3. R. Dashen, "Path Integrals for Waves in Random Media," *J. Math. Phys.*, vol. 20, no. 5, pp. 894-920 (1979).

4. S. M. Flatté, R. Dashen, W. M. Munk, K. M. Watson, and F. Zachariasen, *Sound Transmission through a Fluctuating Ocean*, Cambridge University Press, Cambridge (1979). 299 pages

5. S. M. Flatté, "Wave propagation through random media: contributions from ocean acoustics," *Proceedings of the IEEE*, vol. 71, no. 11, pp. 1267-1294 (1983).

6. S. M. Flatté, S. A. Reynolds, and R. Dashen, "Path-integral treatment of intensity behavior for rays in a sound channel," *J. Acoust. Soc. Am.* (to editor: fill in appropriate reference to companion paper).

7. R. Dashen, S. M. Flatté, and S. A. Reynolds, "Path-integral treatment of acoustic mutual coherence functions for rays in a sound channel," *J. Acoust. Soc. Am.*, vol. 77, no. 5, pp. 1716-1722 (1985).

8. S. A. Reynolds , S. M. Flatté, R. Dashen, B. Buehler, and P. Maciejewski, "AFAR measurements of acoustic mutual coherence functions of time and frequency," *J. Acoust. Soc. Am.*, vol. 77, no. 5, pp. 1723-1731 (1985).

9. P. F. Worcester, G. O. Williams, and S. M. Flatté, "Fluctuations of resolved multipaths at short range in the ocean," *J. Acoust. Soc. Am*, vol. 70, no. 3, pp. 825-840 (1981).

10. T. E. Ewart, "Acoustic fluctuations in the open ocean-A measurement using a fixed refracted path," *J. Acoust. Soc. Am.*, vol. 60, no. 1, pp. 46-59 (1976).

11. T. E. Ewart and S. A. Reynolds, "The Mid-Ocean Acoustic Transmission Experiment -MATE-," *J. Acoust. Soc. Am.*, vol. 75, no. 3, pp. 785-802 (1984).

12. F. Dyson, W. Munk, B. Zetler, "Interpretation of multipath scintillations Eleuthera to Bermuda in terms of internal waves and tides," *J. Acoust. Soc. Am.*, vol. 59, no. 5, pp. 1121-1133 (1976).

13. W. H. Munk and F. Zachariasen, "Sound propagation through a fluctuating, stratified ocean: Theory and observation," *J. Acoust. Soc. Am.*, vol. 59, no. 4. pp. 818-838 (1976).

14. J. Spiesberger and P. Worcester, "Fluctuations of resolved acoustic multipaths at long range in the ocean," *J. Acoust. Soc. Am.*, vol. 70, no. 2, pp. 565-576 (1981).

15. H. A. Deferrari, R. I. Davis, H. Nguygen, R. F. Tusting, and N. J. Williams, "Measurements of transmission fluctuations at three ranges for refracted paths through the deep ocean," *J. Acoust. Soc. Am.*, vol. 74, no. 5, pp. 1448-1463 (1983).

16. W. H. Munk, "Internal waves and small-scale processes," in *Evolution of Physical Oceanography*, ed. B. A. Warren and C. Wunsch, pp. 264-291, MIT Press, Cambridge, MA (1981).

17. M. D. Levine, C. A. Paulson and J. H. Morison, "Internal waves in the Arctic Ocean: a comparison with lower-latitude observations," *J. Physical Oceanog.*, vol. 15, no. 6, pp. 800-809 (1985).

18. R. Dashen, "Distribution of intensity in a multiply scattering medium," *Optics Lett.*, vol. 10, no. 4, pp. 110-112 (1984).

19. S. M. Flatté, D. R. Bernstein, R. Dashen, "Intensity moments by path integral techniques for wave propagation through random media, with application to sound in the ocean," *Physics of Fluids*, vol. 26, no. 7, pp. 1701-1713 (1983).

20. E. Jakeman and P. N. Pusey, "Significance of K-distributions in scattering experiments," *Phys. Rev. Lett.*, vol. 40, no. 9, pp. 546-550 (1978).

21. C. H. Reinsch, "Smoothing by spline functions," *Numerische Mathematik*, vol. 10, pp. 177-183 (1967).

22. R. K. Otnes and L. Enochson, *Applied Time Series Analysis*, Wiley-Interscience, New York (1978).

23. C. C. Macaskill and T. E. Ewart, "The probability distribution of intensity for acoustic propagation in a randomly varying ocean," *J. Acoust. Soc. Am.*, vol. 76, no. 5, pp. 1466-1473 (1984).

TABLE I.

Internal wave model and predicted acoustic parameters at AFAR

Internal Wave Model Parameters	
$\mathcal{S}_0$	13.1 m
j_*	3
$n_0 B$	3 cph km

Acoustic Parameters
(1 cm s^{-1} smoothing of the background profile)

Short Range

σ_0(Hz)	10^3 A	Φ
749.8	2.3	2.8
1499.8	1.2	5.5
2800.0	0.63	10.

Long Range

σ_0(Hz)	10^3 A	Φ	γ	ν (h^{-1})	ν' (h^{-1})
410	47.	7.2	.15	6.4	3.9
1010	19.	18	.11	16.	12.
4670	4.2	82.	.064	73.	67.

TABLE II.

Observed and predicted moments $\langle I^N \rangle / \langle I \rangle^N$ at 35 km

N =	2	3	4	5	6
410 Hz	±0.26	±2.1			
Observed	2.24	8.5	47.6	339	2780
equation (6)	2.24	8.5	48	380	4000
equation (7)	2.24	8.2	41	264	2000
equation (8)	2.24	8.3	45	335	3200
1010 Hz					
Observed	2.21	8.22	43.5	290	2240
equation (6)	2.21	8.3	46	360	3700
equation (7)	2.21	8.0	40	250	1900
equation (8)	2.21	8.1	44	310	2900
4670 Hz					
Observed	2.47	11.0	74.3	658	6900
equation (6)	2.47	11	85	990	17000
equation (7)	2.47	10	58	402	3260
equation (8)	2.47	11	74	721	9400

FIG. 1. The $\Lambda - \Phi$ diagram for AFAR. The points in the unsaturated regime, $\Lambda\Phi^2 < 1$, are from the 2.8 km experiment. The points in the partially saturated regime, $\Lambda\Phi^2 > 1$ and $\Lambda\Phi < 1$ are for the different acoustic frequencies over the 35-km path. The fully saturated area is $\Lambda\Phi > 1$.

FIG. 2. (a) The intensity series at 2.8 km. The interval between tick marks is 5 times the mean intensity. The series are for 750 Hz (top trace), 1500 Hz (middle trace), and 2800 Hz (bottom trace). (b) 20 hours of intensity data for three frequencies over the 35-km path. The interval between tick marks is 10 times the mean intensity. The acoustic frequencies are 410 Hz (top), 1010 Hz (middle) and 4671 Hz (bottom).

FIG. 3. Observed intensity correlation (dots, with occasional error bars indicated) in the form of equation (1) for 1010 Hz compared with $K(\Delta t)$ calculated using two smoothings: dy = 1.5 and 1.0 cm/s. The $e^{-(\nu'\Delta t)^2}$ curve is also shown. The $|Q|^2$ curve comes from an approximation to $K(\Delta t)$ involving the two-frequency second moment. [6]

FIG. 4. Intensity correlation functions at 35 km; the dotted curves are experimental data, the solid curves are the theoretical predictions; 90% confidence intervals are shown for a few lags.

FIG. 5. Normalized power spectra of intensity at 35 km compared with the prediction from the Fourier transform of $K(\Delta t)$. Power spectra with 90% confidence intervals centered at 10^{-4} are shown on the 410-Hz graph. The almost vertical extra line segments at high frequency are the tails of the predictions from the Fourier transforms of $e^{-(\nu'\Delta t)^2}$.

FIG. 6. As in Figure 5, plotted so that equal areas under the curves correspond to equal contributions to the variance.

FIG. 7. The correlation of intensity as a function of frequency difference at 3200 Hz over the 35 km path. The dots are experimental data and the solid curve is the thoeretical prediction. The dashed curve shows the prediction obtained by setting $U_o'' = 0$: that is, ignoring the sound channel.

FIG. 8. The correlation of intensity as a function of time lag within the pulse. The dots are experimental data; the solid curve is from a full calculation of $Q(\Delta\sigma)$, that is, (14); the dashed curve is from the Gaussian approximation to $Q(\Delta\sigma)$, that is, (16).

FIG. 9. Probability densities for log-intensity calculated from 35-minute segments for the three frequencies at 2.8 km. 90% confidence intervals are shown (every other interval for 750 Hz). Normal curves with mean and variance from the data are plotted as solid lines.

FIG. 10. Probability densities for normalized intensity at 35 km. 90% confidence intervals are shown. Exponential distributions are shown as solid straight lines. K-distributions with γ's from the observed values of $\langle I^2 \rangle$ are shown as solid curves.

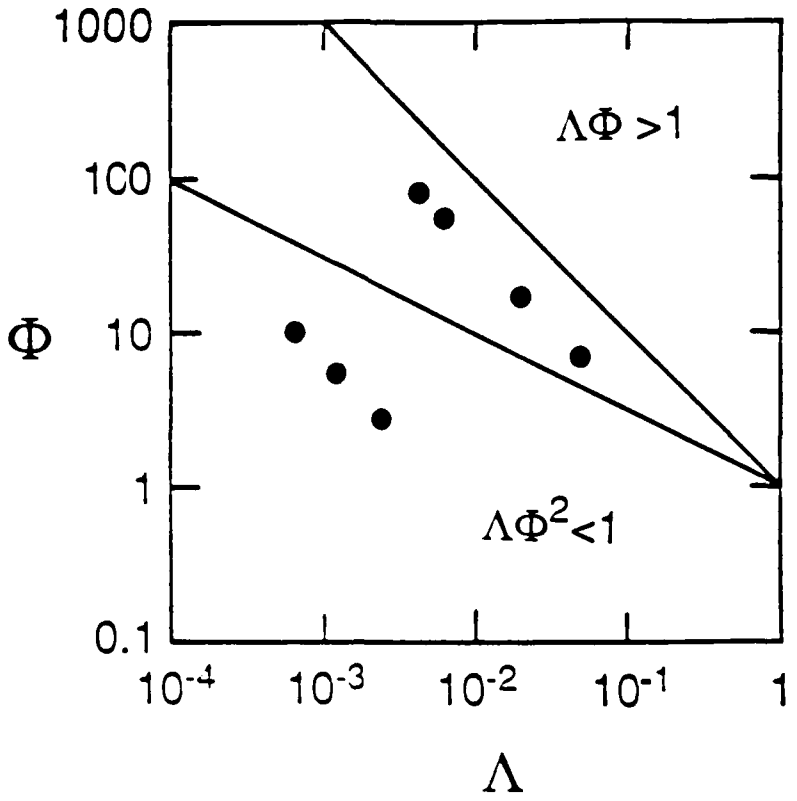

FIG. 1. The $\Lambda - \Phi$ diagram for AFAR. The points in the unsaturated regime, $\Lambda\Phi^2<1$, are from the 2.8 km experiment. The points in the partially saturated regime, $\Lambda\Phi^2>1$ and $\Lambda\Phi<1$ are for the different acoustic frequencies over the 35-km path. The fully saturated area is $\Lambda\Phi>1$

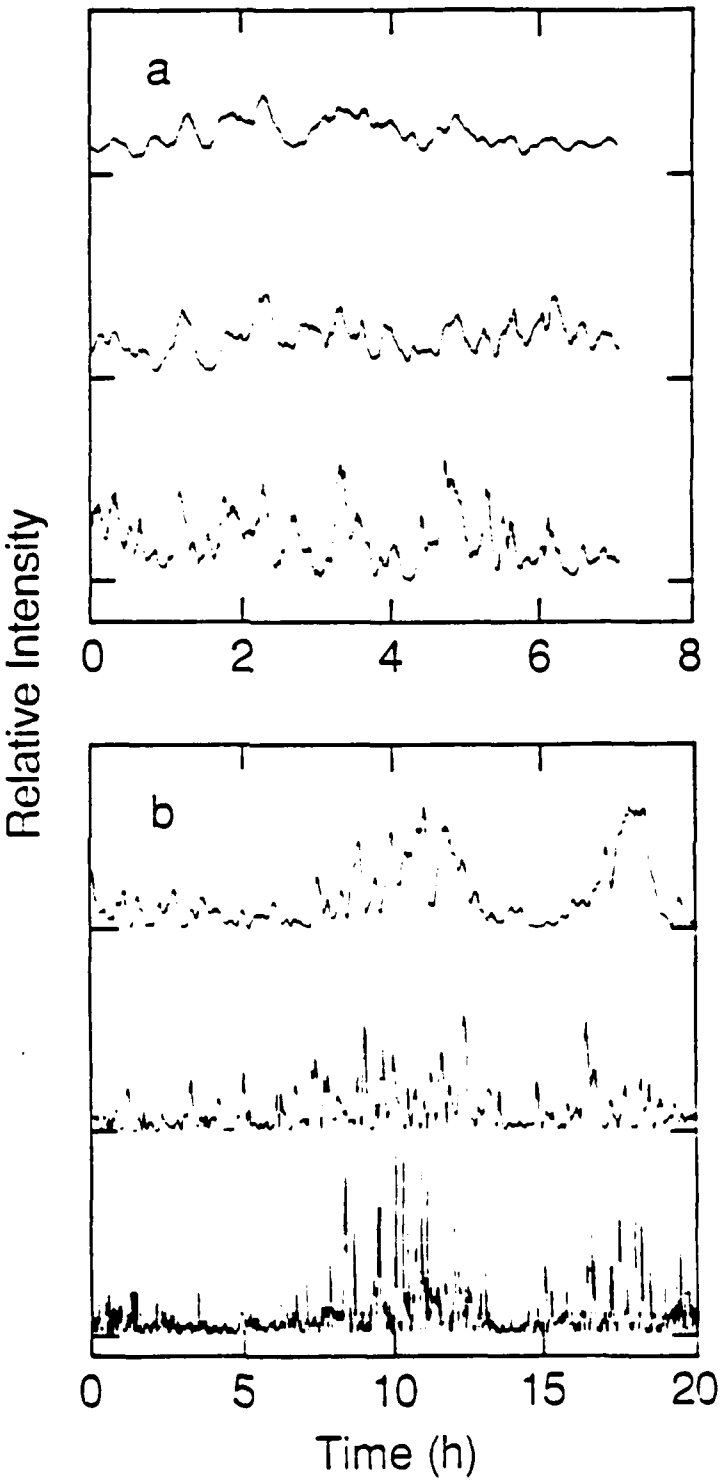

FIG. 2. (a) The intensity series at 2.8 km. The interval between tick marks is 5 times the mean intensity. The series are for 750 Hz (top trace), 1500 Hz (middle trace), and 2800 Hz (bottom trace). (b) 20 hours of intensity data for three frequencies over the 35-km path. The interval between tick marks is 10 times the mean intensity. The acoustic frequencies are 410 Hz (top), 1010 Hz (middle) and 4671 Hz (bottom).

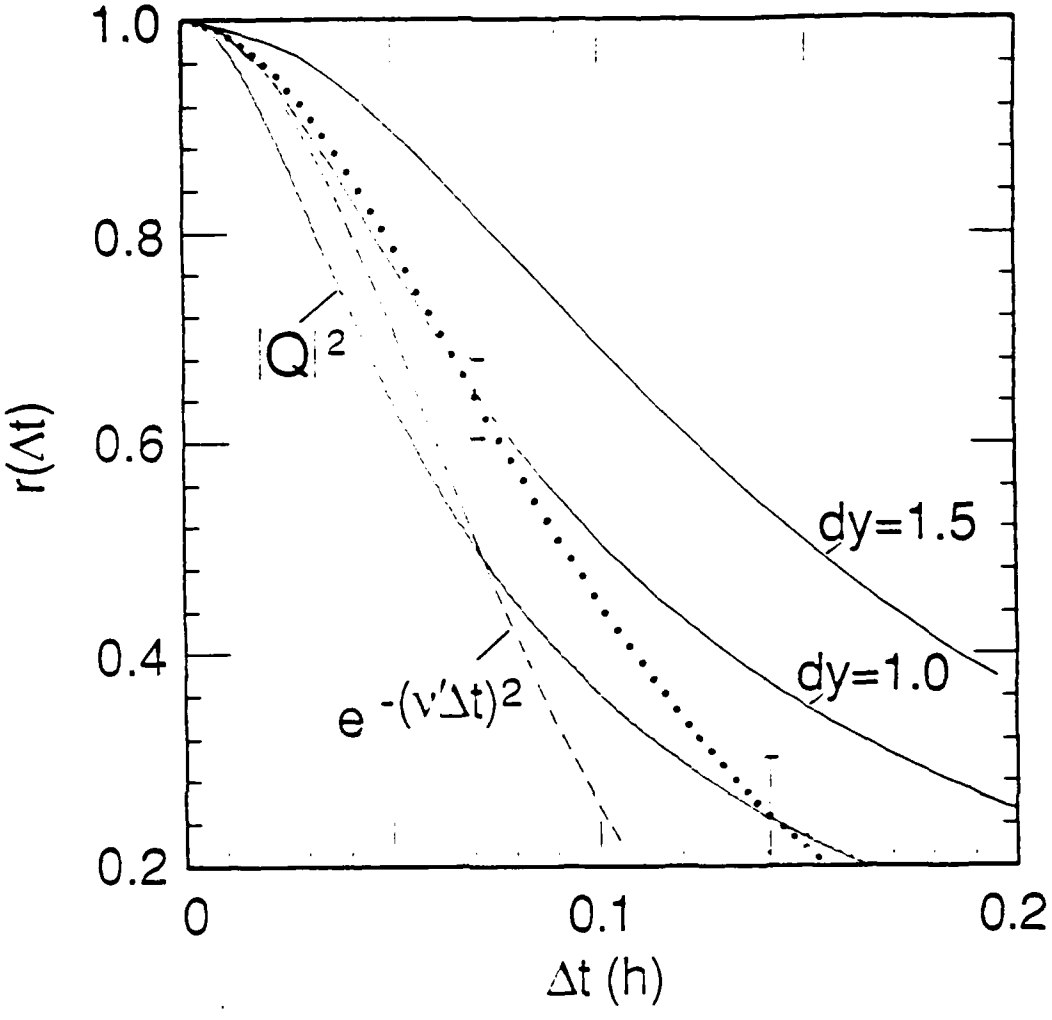

FIG. 3. Observed intensity correlation (dots. with occasional error bars indicated) in the form of equation (1) for 1010 Hz compared with K(Δt) calculated using two smoothings: dy = 1.5 and 1.0 cm/s. The $e^{-(\nu'\Delta t)^2}$ curve is also shown. The $|Q|^2$ curve comes from an approximation to K (Δt) involving the two-frequency second moment. [6]

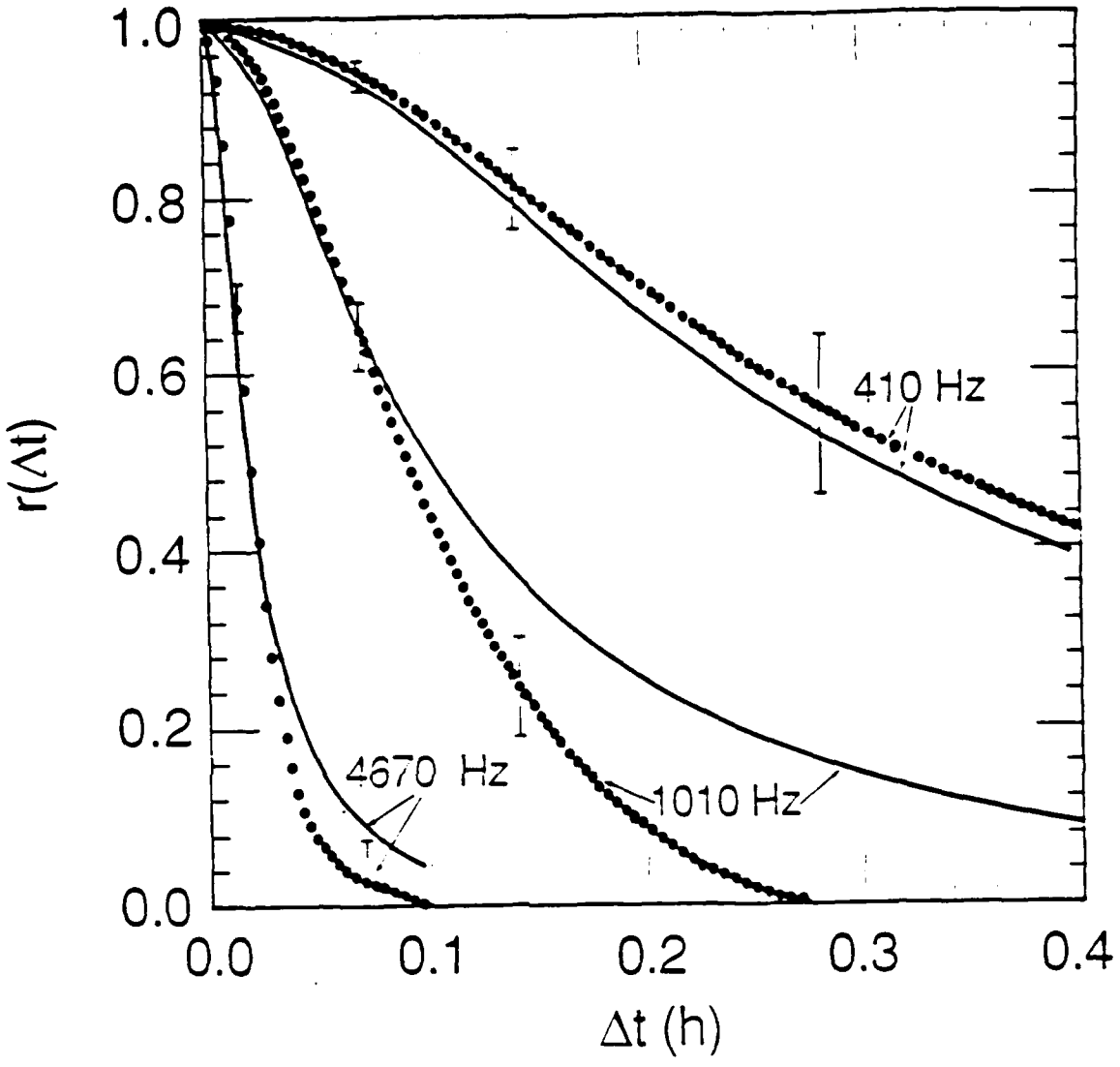

FIG. 4. Intensity correlation functions at 35 km: the dotted curves are experimental data, the solid curves are the theoretical predictions; 90% confidence intervals are shown for a few lags.

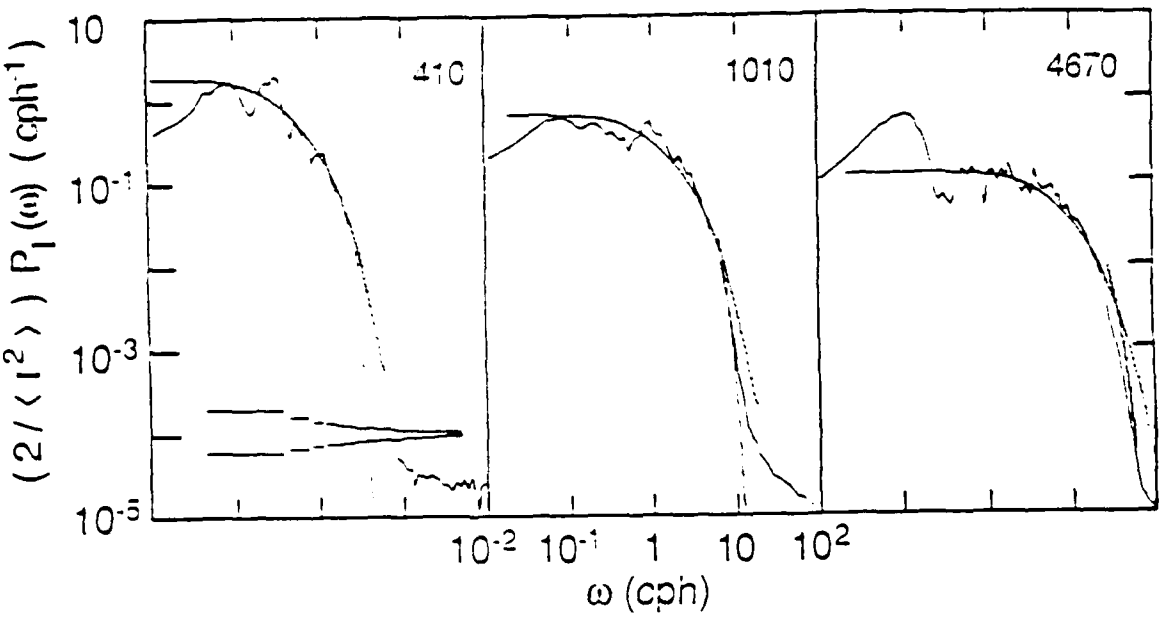

FIG. 5. Normalized power spectra of intensity at 35 km compared with the prediction from the Fourier transform of $K(\Delta t)$. Power spectra with 90% confidence intervals centered at 10^{-4} are shown on the 410-Hz graph. The almost vertical extra line segments at high frequency are the tails of the predictions from the Fourier transforms of $e^{-(\nu'\Delta t)^2}$.

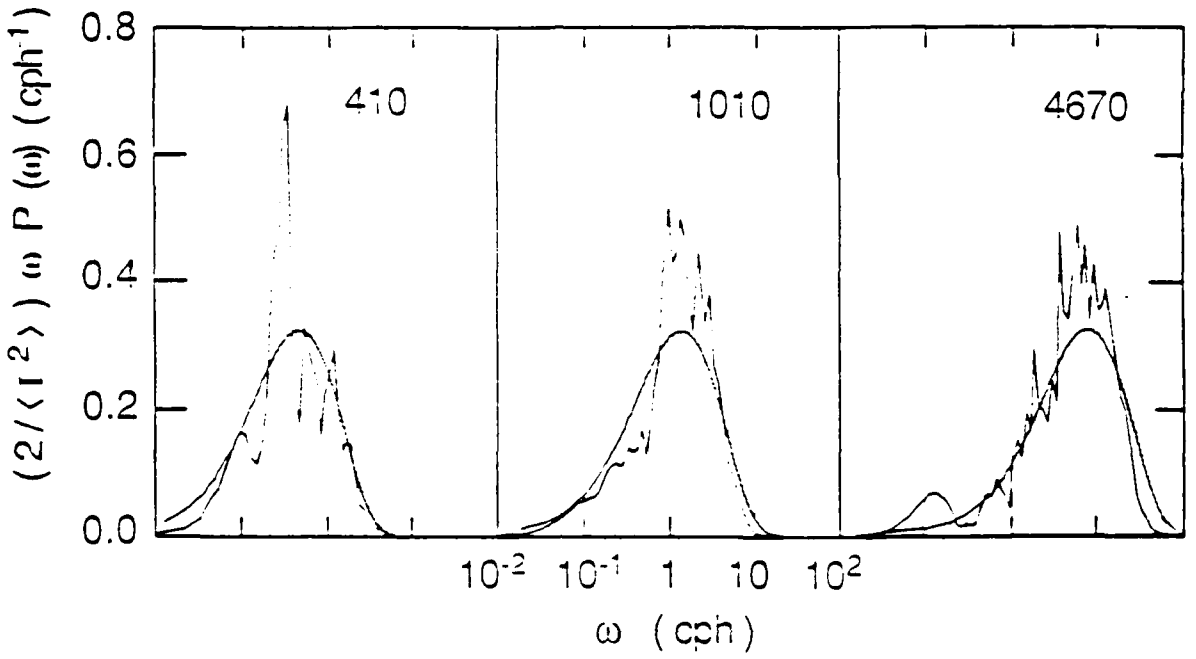

FIG. 6. As in Figure 5, plotted so that equal areas under the curves correspond to equal contributions to the variance.

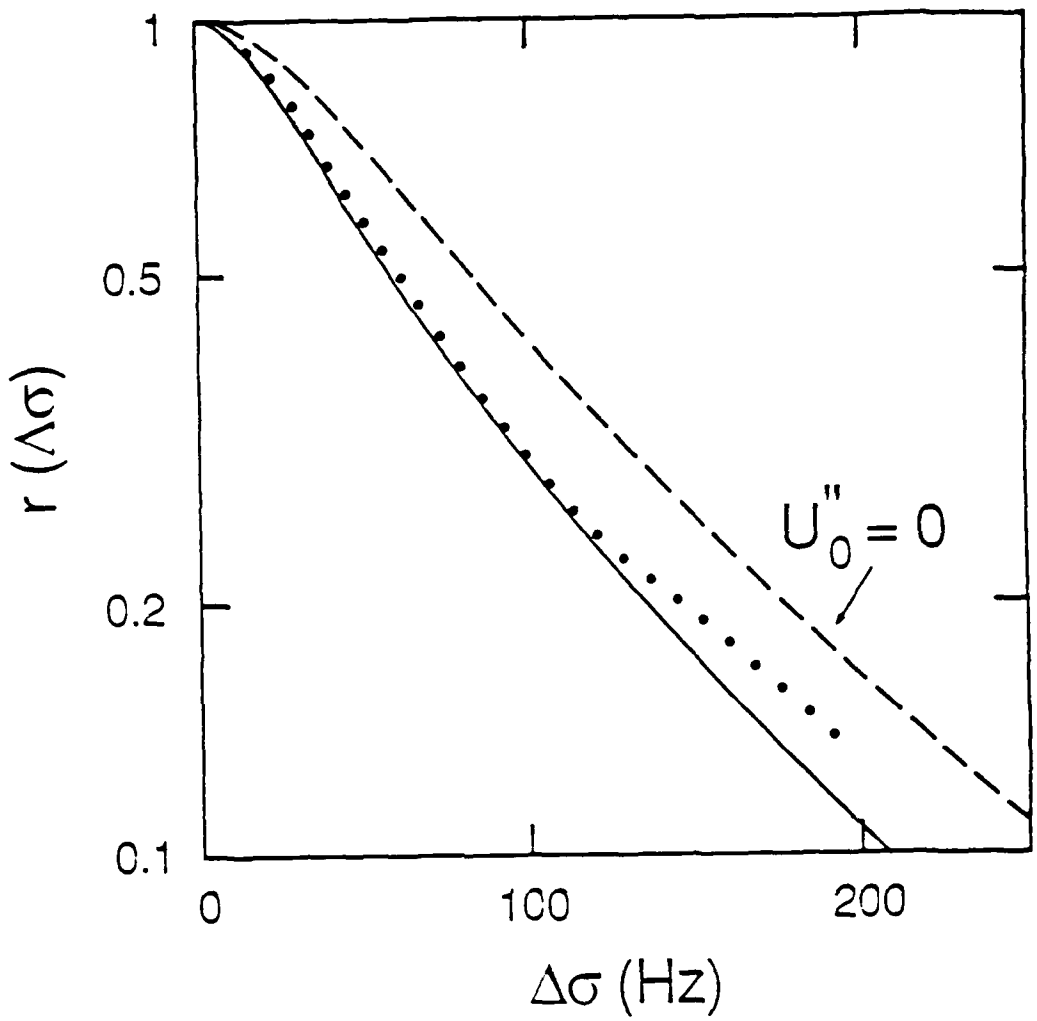

FIG. 7. The correlation of intensity as a function of frequency difference at 3200 Hz over the 35 km path. The dots are experimental data and the solid curve is the thoeretical prediction. The dashed curve shows the prediction obtained by setting $U_o'' = 0$: that is, ignoring the sound channel.

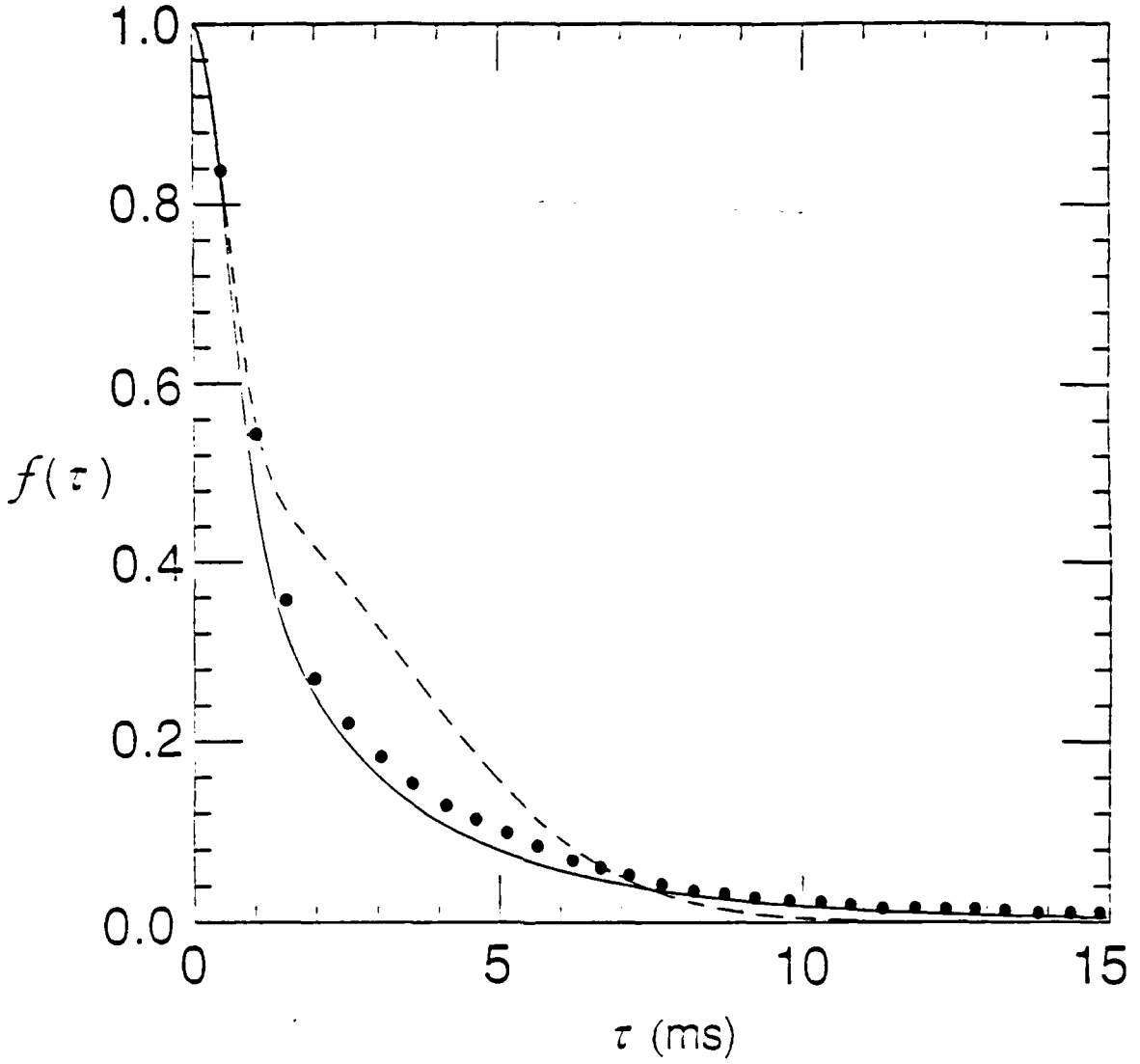

FIG. 8. The correlation of intensity as a function of time lag within the pulse. The dots are experimental data; the solid curve is from a full calculation of Q ($\Delta\sigma$), that is, (14); the dashed curve is from the Gaussian approximation to Q ($\Delta\sigma$), that is, (16).

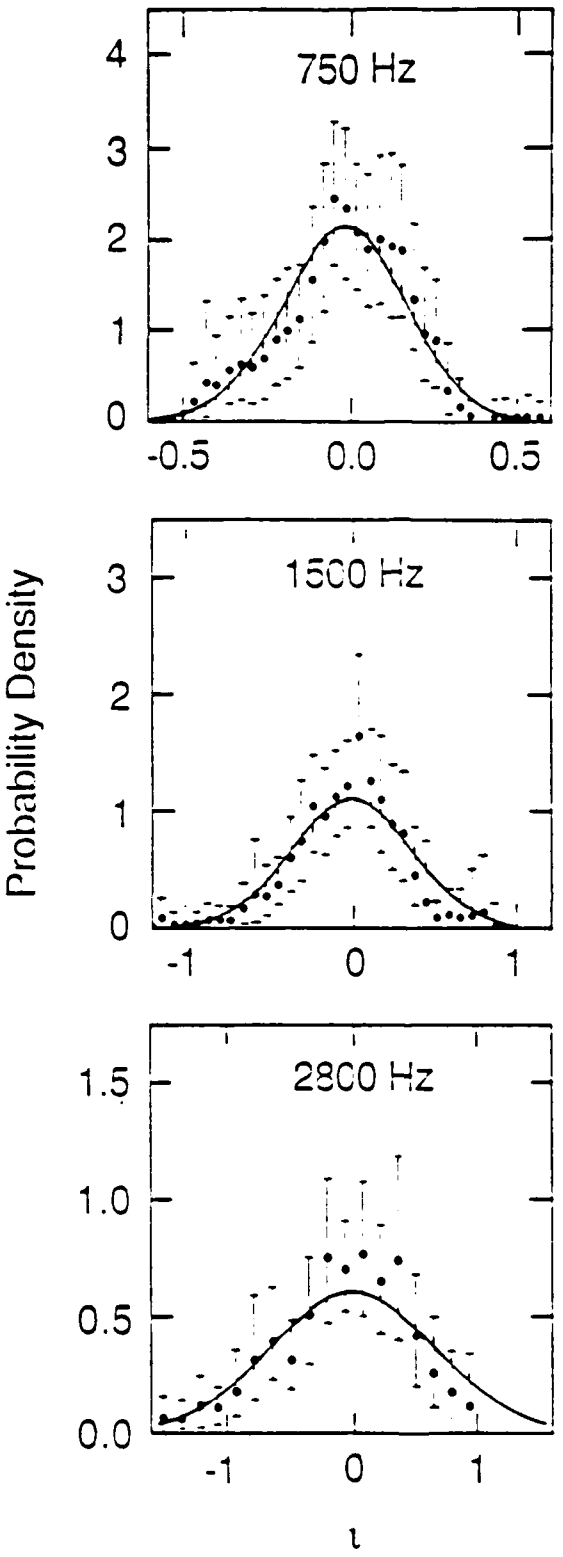

FIG. 9. Probability densities for log-intensity calculated from 35-minute segments for the three frequencies at 2.8 km. 90% confidence intervals are shown (every other interval for 750 Hz). Normal curves with mean and variance from the data are plotted as solid lines.

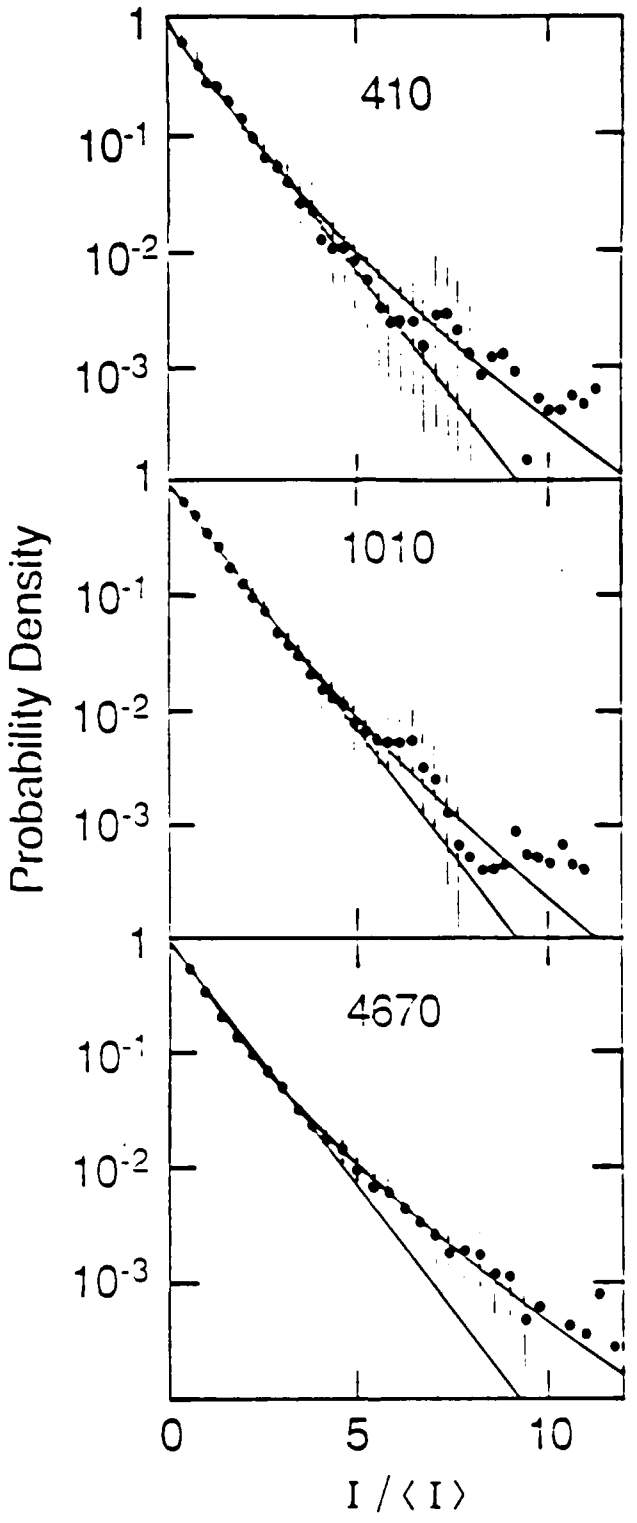

FIG. 10. Probability densities for normalized intensity at 35 km. 90% confidence intervals are shown. Exponential distributions are shown as solid straight lines. K-distributions with γ's from the observed values of $\langle I^2 \rangle$ are shown as solid curves.

END

10-87

DTIC